Collective excitations of a quantized vortex in $^3P_2$ superfluids in neutron stars

Chandrasekhar Chatterjee,[1,*] Mareike Haberichter,[1,2,3,†] and Muneto Nitta[1,‡]

[1]*Department of Physics, and Research and Education Center for Natural Sciences, Keio University, Hiyoshi 4-1-1, Yokohama, Kanagawa 223-8521, Japan*

[2]*Institut für Physik, Universität Oldenburg, Postfach 2503 D-26111 Oldenburg, Germany*

[3]*Department of Mathematics and Statistics, University of Massachusetts, Amherst, Massachusetts 01003-4515, USA*

(Dated: December 19, 2016)

We discuss collective excitations (both fundamental and solitonic excitations) of quantized superfluid vortices in neutron $^3P_2$ superfluids, which likely exist in high density neutron matter such as neutron stars. Besides the well-known Kelvin modes (translational zero modes), we find a gapfull mode whose low-energy description takes the simple form of a double sine-Gordon model. The associated kink solution and its effects on spontaneous magnetization inside the vortex core are analyzed in detail.

arXiv:1612.05588v1 [nucl-th] 16 Dec 2016

I. INTRODUCTION

The properties of high density nuclear matter are still not sufficiently understood. However, in recent years, neutron star (NS) observations began to place stronger restrictions [1–3] on the equation of state (EoS) of dense matter and to probe structure and composition of NS cores. Most valuable information into the state of their interiors came from the detections of pulsar glitches via pulsar timing measurements, optical and X-ray observations of cooling and accreting NSs and from neutrino emission measurements from proto-neutron stars. These observations provide evidence for superfluidity in the interiors of NSs [4].

The first direct evidence [5, 6] that the NS core should exist in a superfluid state has been reported in the study of the NS in the supernova remnant known as Cassiopeia A. It has been measured that Cassiopeia A's surface temperature has rapidly decreased from 2.12×10^6 K to 2.04×10^6 K. This pronounced drop in surface temperature can be naturally explained [5–7] if one assumes that neutrons have recently become superfluid in the NS core. As the neutrons combine to form Cooper pairs, a splash of neutrinos is emitted accelerating the NS cooling process. Another evidence for a superfluid NS core comes from the observation of pulsar glitches, which are sudden jumps in the NS rotation frequency. Glitches like the ones observed in the Crab and Velar pulsar can be explained by two main physical mechanism – either they are due to starquakes from the NS core [8, 9] or crust [10–12] or they are caused by the sudden unpinning and displacement of a large number of vortices [11–13] in the NS superfluid. In the starquake glitch model [12, 14, 15], the glitches are caused by a sudden reduction in the moment of inertia of some solid component of the NS. For example, the differential rotation between the crust and the superfluid NS core can produce stresses [12] in the NS crust leading to crustquakes. The resulting crustquakes distort the star's shape and hence generate sudden jumps in the NS rotational frequency, seen as glitches. In contrast, in the pinned superfluid model angular momentum is suddenly transferred from the superfluid NS core to the non-superfluid crust via vortex unpinning, spinning it up. Neutron superfluid vortices can become pinned to nuclear clusters in the inner crust [11] or to magnetic flux tubes in the core [16]. This prevents angular momentum from being transferred to the NS crust. Hence, a differential rotation builds up between the NS core and crust. When this differential becomes large enough angular momentum is suddenly transferred from the core to the crust through the catastrophic unpinning of vortices, resulting in a sudden spin-up in the NS. Furthermore, the observed long time relaxation after glitches can be explained only by assuming the coexistence of normal and superfluid components [8, 10]. Therefore, understanding the properties of neutron superfluidity and the formation and dynamics of superfluid vortices can give us further insights into the evolution of NSs and their composition.

At the high density central part of NSs the neutron superfluidity is attributed to the $^3P_2$ pairing interaction [17–22] rather than to $^1S_0$ pairing familiar from the conventional BCS theory of superconductors. Analysis of nucleon-nucleon scattering data [18] shows that the transition from an isotropic $^1S_0$ superfluid to an anisotropic $^3P_2$ superfluid occurs at densities above $1.6\times10^{14}\,g/\mathrm{cm}^3$. The Ginzburg-Landau (GL) energy functional generalized for $^3P_2$ superfluids was developed in Refs. [21, 22] in the weak coupling limit. Note that the general GL free energy formally agrees with the angular momen-

* chandra@phys-h.keio.ac.jp
† mareike@math.umass.edu
‡ nitta@phys-h.keio.ac.jp

tum $l = 2$ GL functional solved by Mermin [23]; depending on the GL parameters, the ground state is in either nematic, ferromagnetic or cyclic phase. The ground states of $^3P_2$ superfluids in the weak coupling limit were found in Ref. [24] to be in the nematic phase in the absence of a magnetic field. They are continuously degenerated when we ignore the sixth order term and can be decomposed by unbroken $O(2)$, D_2 and D_4 symmetry groups into the uniaxial, D_2- and D_4-biaxial nematic phases, respectively. (This is also known from spin-2 spinor Bose-Einstein condensates, see Refs. [25, 26].) This degeneracy is lifted and the uniaxial nematic phase becomes the unique ground state once the sixth order term is taken into account. The ground states in the presence of a magnetic field were recently determined [27]; the ground state is in the uniaxial nematic phase for smaller magnetic fields relevant for ordinary NSs and in the D_2- or D_4-biaxial nematic phase for large magnetic field relevant for magnetars. Beyond the GL theory, the ground states in the (T,H) phase diagram have been obtained recently in the Bogoliubov-de Gennes (BdG) formalism [28]. The D_2- and D_4-biaxial nematic phases appear in lower T and H region and in higher T and H region, respectively. The phase boundary is of second order at higher temperature while it is of first order at lower temperature, and a tricritical point connects these boundaries. One of the most important results of the BdG formalism is that $^3P_2$ superfluids were found to be topological superfluids predicting gapless Majorana fermions on the surface [28]. The strong-coupling corrections to the $^3P_2$ NS matter GL free energy including spin-orbit and central forces were calculated in Ref. [29].

As phenomenological aspects relevant for NSs physics are concerned, $^3P_2$ superfluids provide new mechanisms for neutrino emission of dense neutron matter [30–39], explain the entrainment [40] of superconducting protons by rotating superfluid neutrons in NSs and offer possible explanations of the anomalously rapid cooling of NSs [5–7].

Since superfluids are rotating inside NSs, a large number ($\sim 10^{19}$) of superfluid vortices exist in their interior. The rich structure and magnetic properties of vortices emerging in the GL equations for $^3P_2$ superfluids were explored in Refs. [22, 27, 41–43]. $^3P_2$ vortices in NS matter turn out to be structurally different from their counterparts in $^1S_0$ superfluids. For example, different to $^1S_0$ vortices, $^3P_2$ vortices exhibit spontaneous magnetization in the vortex core region [27, 42]. For magnetic field strengths of orders of magnitude as they appear in magnetars, the ground state is in the D_4-biaxial nematic phase, in which the first homotopy group π_1 is non-Abelian, thereby admitting non-Abelian (non-commutative) vortices which carry half-quantized circulation [43].

In this article, we study low-energy collective modes [or (pseudo) moduli] and solitonic excitations of an integer vortex in a $^3P_2$ superfluid. By solving numerically the GL equation, we reconstruct the axially symmetric integer vortex solution in the absence of magnetic fields and sixth order terms. Because of the off-diagonal elements of the tensor order parameter, there exists spontaneous magnetization at the vortex core as described above. Here, we calculate the net magnetic moment per femtometer along vortex line to be one order less than the neutron magnetic moment. We then study collective modes in the presence of a single vortex. As usual, there are gapless (massless) Kelvin modes (translational moduli) due to the spontaneously broken translational symmetry in the presence of the vortex. In addition, the phase δ of the off-diagonal elements of the tensor order parameter gives rise to a gapfull (massive) mode. We construct the low-energy (long distance) effective free energy of this gapfull mode and find it is a double sine-Gordon model, consisting of the potential terms $\cos\delta$ and $\cos 2\delta$. For GL parameter values describing typical NSs, it allows only 2π kink solutions [44]. We find that the core magnetization of the vortex flips its direction at the kink.

The article is structured as follows. After introducing the GL free energy relevant for $^3P_2$ superfluids in the weak coupling limit, $^3P_2$ vortex solutions are constructed in Section II and their spontaneous magnetization in the vortex core region is evaluated. Then, in Section III, we discuss the effect of the parameter δ on the free energy density by writing down the associated effective free energy functional which takes the simple form of a double sine-Gordon model. The associated kink soliton solution is derived in Section IV. Finally, our conclusions and possible future lines of investigation are presented in Section V. To facilitate the reader to reproduce our numerical results, we add two appendices to this article. In Appendix A, we briefly review the GL theory for $^3P_2$ superfluid states and state all the parameter values used in our numerical simulations. We list explicitly all the vortex equations together with the imposed boundary conditions in Appendix B. Note that a detailed investigation of vortex structure and dynamics in the presence of nonzero external magnetic fields and higher order terms, in particular the inclusion of the sixth order term, will be published in a forthcoming paper.

II. GINZBURG-LANDAU DESCRIPTION OF VORTICES IN $^3P_2$ NEUTRON SUPERFLUIDS

In this section we discuss the GL free energy and determine the vortex configurations numerically. A discussion of spontaneous magnetization is included at the end of the section.

A. Ginzburg-Landau Free Energy

The GL free energy for the $^3P_2$ superfluidity was originally derived in Refs. [22, 42, 43, 45] by generalizing Gor'kov's procedure. In this case the original $^1S_0$ contact interaction was generalised to a $^3P_2$ contact interaction by introducing a derivative coupling. A short explanation of the derivation is given in Appendix A.

The tensorial order parameter $A_{\mu i}$ transforms under the symmetry group as

$$A \to e^{i\theta} \boldsymbol{g} A \boldsymbol{g}^T, \quad \text{with} \quad e^{i\theta} \in U(1), \quad \text{and} \quad \boldsymbol{g} \in SO(3)_{L+S}. \tag{II.1}$$

Here, $SO(3)_{L+S}$ is the diagonal subgroup of the full group $SO(3)_L \times SO(3)_S$ and is generated by the total angular momentum $J = L + S$.

The GL free energy density F can be written as a function of the tensor $A_{\mu i}$

$$F = \frac{1}{G} \int d^3\rho \ \left(F_{\text{grad}} + F_{2+4} + F_6 + F_H \right), \tag{II.2}$$

where F_{grad} is the gradient term, F_{2+4} and F_6 [46] are the free energy densities up to fourth order and up to sixth order, respectively and F_H is the magnetic term. Here, we rescaled for later convenience the free energy functional by $G = 3\pi^2/\left(m_n k_F^3\right) \approx 115.39\,\text{MeV}\,\text{fm}^5$ where k_F is the Fermi momentum and m_n represents the nucleon mass, see Appendix A for the numerical values of all model parameters. The free energy density contributions are explicitly given by

$$F_{\text{grad}} = K_1\, \partial_i A_{\mu j} \partial_i A^\dagger_{\mu j} + K_2 \left(\partial_i A_{\mu i} \partial_j A^\dagger_{\mu j} + \partial_i A_{\mu j} \partial_j A^\dagger_{\mu i} \right), \tag{II.3a}$$

$$F_{2+4} = \alpha\, \text{Tr} AA^\dagger + \beta \left[\left(\text{Tr} AA^\dagger \right)^2 - \text{Tr} A^2 A^{\dagger 2} \right], \tag{II.3b}$$

$$\begin{aligned} F_6 =& \gamma_6 \left[-3 \left(\text{Tr} AA^\dagger \right) |\text{Tr} AA|^2 + 4 (\text{Tr} AA^\dagger)^3 \right. \\ & + 12 (\text{Tr} AA^\dagger) \text{Tr} (AA^\dagger)^2 + 6 (\text{Tr} AA^\dagger) \text{Tr} (A^2 A^{\dagger 2}) \\ & + 8 \text{Tr} (AA^\dagger)^3 + 12 \text{Tr} [(AA^\dagger)^2 A^\dagger A] \\ & \left. - 12 \text{Tr} [AA^\dagger A^\dagger A^\dagger AA] - 12 \text{Tr} AA (\text{Tr} AA^\dagger AA)^* \right], \end{aligned} \tag{II.3c}$$

$$F_H = g'_H H^2 \text{Tr} \left(AA^\dagger \right) + g_H H_\mu \left(AA^\dagger \right)_{\mu\nu} H_\nu, \tag{II.3d}$$

where H is the strength of the external magnetic field and we implicitly sum over repeated indices. Note that for simplicity, we set $g'_H = 0$ in Eq. (II.3d). In this paper we also neglect the sixth order term because of small values of γ_6. Existence of nonzero γ_6 would make our system metastable, however we assume that small value of γ_6 would make the relaxation time much longer than the time scale of the system.

B. Vortex Configuration

Vortex configurations in the absence of a magnetic field and sixth order terms were first studied in Refs. [22, 41]. Since the order parameter is tensorial, we have to choose a basis which diagonalizes the tensor. In Refs. [22, 41], the configuration in which the tensor is diagonalized in the cylindrical basis was considered. One interesting feature is that the continuos degeneracy of the ground state is lifted in the presence of a vortex. Later, this configuration was compared with the configuration in which the tensor is diagonalized in the Cartesian basis, and it was confirmed that the former gives the lowest energy configuration [27].

In this subsection, we shall derive the equations of motion for the vortex profile functions using the following ansatz [27] for the order parameter of a vortex state

$$\begin{aligned} A^{(x,y,z)} &= \sqrt{\frac{|\alpha|}{6\beta}} R(\theta) A^{(\rho,\theta,z)} R^T(\theta) e^{i\theta}, \\ A^{(\rho,\theta,z)} &= \begin{pmatrix} f_1 & ige^{i\delta} & 0 \\ ige^{i\delta} & f_2 & 0 \\ 0 & 0 & -f_1 - f_2 \end{pmatrix}, \end{aligned} \tag{II.4}$$

where (ρ, θ, z) denote cylindrical coordinates and δ is a constant parameter. $A^{(x,y,z)}$ is the order parameters in the Cartesian basis and $A^{(\rho,\theta,z)}$ is the order parameters in the cylindrical basis which are related by a rotation matrix R, given by

$$R(\theta) = \begin{pmatrix} \cos\theta & -\sin\theta & 0 \\ \sin\theta & \cos\theta & 0 \\ 0 & 0 & 1 \end{pmatrix}. \tag{II.5}$$

Here, f_1, f_2 and g are profile functions depending only on the radial coordinate ρ, and satisfying the boundary conditions

$$\begin{aligned} f_1, f_2 \to r, \quad g \to 0 \qquad & \text{as } \rho \to \infty, \\ f_1, f_2 \to 0, \quad g \to 0 \qquad & \text{as } \rho \to 0. \end{aligned} \tag{II.6}$$

The boundary condition at spatial infinity is determined by energy minimization to be given by $r = 6 - \sqrt{43} \sim -0.557$ [22, 27, 41]; the continuous degeneracy of the ground state is lifted in the vortex background as described above.

As the profile function g vanishes at the origin and at spatial infinity, it creates ring-shaped soliton solutions and in general one may replace g by $ge^{im\theta}$, where m denotes how many times the phase of g is twisted along the ring. Note that in Ref. [47] winding numbers that are locally defined in the core region were used to classify vortex-core structures in spin-1 Bose-Einstein condensates.

Using the ansatz (II.4) we may rewrite the free energy (II.2) as

$$F = \int \mathrm{d}^2\rho \, \frac{|\alpha|}{6\beta}\frac{K}{G}\left\{(t_1+t_2)+\frac{\alpha}{K}t_3+\frac{|\alpha|}{6K}t_4\right\}, \qquad \text{(II.7)}$$

where the individual energy density contributions t_1, t_2, t_3 and t_4 take the following form

$$t_1 = 2\left(f_1'^2+f_2'^2+f_1'f_2'+g'^2\right)+\frac{1}{\rho^2}\left(4f_1^2+4f_2^2-2f_1f_2+10g^2 - 8(f_1-f_2)g\cos\delta\right), \qquad \text{(II.8a)}$$

$$t_2 = 2\left(f_1'^2+g'^2\right)+\frac{2}{\rho^2}\left\{f_2^2+5g^2+(f_1-f_2)^2 - 2g(f_1-f_2)\cos\delta+4f_2g\cos\delta\right\}+\frac{1}{\rho}\left\{-2\left(f_1'+f_2'\right)g\cos\delta +2(f_1+f_2)g'\cos\delta+2\left(f_1'+f_2'\right)(f_1-f_2)\right\},$$

$$t_3 = 2\left(f_1^2+f_2^2+f_1f_2+g^2\right), \qquad \text{(II.8b)}$$

$$t_4 = 2f_1^4+4f_1^3f_2+6f_1^2f_2^2+4f_1f_2^3+2f_2^4+\{(6+2\cos 2\delta)f_1^2 +4f_1f_2+(6+2\cos 2\delta)f_2^2+4f_1f_2\}g^2+2g^4. \qquad \text{(II.8c)}$$

Here the prime denotes the derivative with respect to ρ. For numerical calculations it is useful to rescale the radial coordinate by $\rho\to\tilde\rho=\rho/\xi$ where $1/\xi^2=12|\alpha|/K$ is the coherence length (~ 30 fm) and to change variables to $u=f_1+f_2$ and $v=f_1-f_2$. After rescaling and change of variables, the free energy (II.7) can be written as

$$F = \int \mathrm{d}^2\tilde\rho \, \frac{2|\alpha|^2\xi^2}{G\beta}\left\{(\tilde t_1+\tilde t_2)+\frac{\alpha}{12|\alpha|}t_3+\frac{1}{72}t_4\right\} \qquad \text{(II.9)}$$

where the energy contributions read

$$\tilde t_1 = \frac{3}{2}u'^2+\frac{1}{2}v'^2+2g'^2+\frac{1}{\tilde\rho^2}\left(\frac{3}{2}u^2+\frac{5}{2}v^2+10g^2-8vg\cos\delta\right), \qquad \text{(II.10a)}$$

$$\tilde t_2 = \frac{1}{2}\left(u'+v'\right)^2+2g'^2+\frac{1}{\tilde\rho^2}\left(\frac{1}{2}u^2+\frac{5}{2}v^2-uv+10g^2 +4g(u-2v)\cos\delta\right)+\frac{1}{\tilde\rho}\left(2(ug'-gu')\cos\delta+2u'v\right), \qquad \text{(II.10b)}$$

$$t_3 = \frac{3}{2}u^2+\frac{1}{2}v^2+2g^2, \qquad \text{(II.10c)}$$

$$t_4 = \frac{1}{8}\left(3u^2+v^2\right)^2+\left[(4u^2+2v^2)+(u^2+v^2)\cos 2\delta\right]g^2+2g^4. \qquad \text{(II.10d)}$$

Here, the prime denotes the derivative with respect to $\tilde\rho$. Note that $\tilde t_1=\xi^2 t_1(\rho)=t_1(\rho/\xi)$. In the following, we calculate the static vortex solution for $\delta=0$. In the next section, the resulting vortex profile functions will be used to study perturbatively the effects of nonzero δ. We summarise the equations of motion derived from the free energy functional (II.9) for vanishing δ together with the imposed boundary conditions in Appendix B.

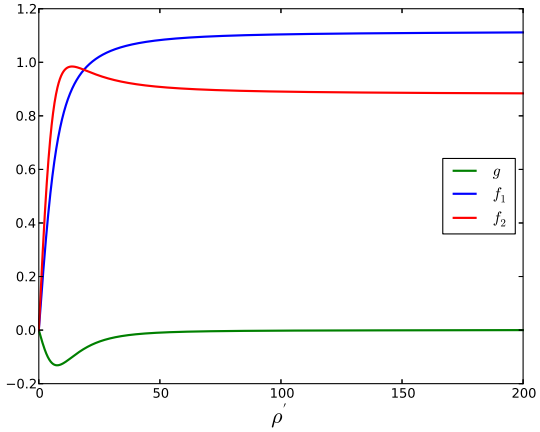

FIG. 1. We display the profile functions f_1, f_2 and g as a function of the distance $\tilde\rho$ from the vortex center. Here, the lowest energy state is in the cylindrical basis ($n=1$) and $r=-0.557$ is selected as the vortex boundary state. Numerical results are shown for the case $m=0$.

The obtained profile functions f_1, f_2 and g are displayed in Fig. 1 as a function of the rescaled radial distance $\tilde\rho$ from the vortex center. To obtain solutions such as those shown in Fig. 1, we solve the equations of motion (B.1) with the boundary conditions stated in Eqs. (B.2) using a numerical relaxation method. The minimal energy solutions in the model (II.9) are constructed by solving the gradient flow equations with a crude initial guess (an approximation in terms of the hyperbolic tangents for the functions u and v and a gaussian curve approximation for the profile function g). The initial configurations are relaxed on a spatial grid with 2001 points and spacing $\Delta\tilde\rho=0.1$.

$^3P_2$ vortices are known to differ from their counterparts in $^1S_0$ superfluids by their nonzero magnetic moments [27, 42]. From the vortex profile functions displayed in Fig. 1, we can compute the resulting small spontaneous magnetization in the $^3P_2$ vortex core region.

The vortex magnetization is given in Refs. [27, 42] by

$$\boldsymbol{M} = \frac{\gamma_n\hbar}{2}\boldsymbol{\sigma}, \qquad \text{(II.11)}$$

where $\boldsymbol{\sigma}$ is computed as

$$\boldsymbol{\sigma} = C_m\frac{|\alpha|}{6\beta}g(\rho)\left[f_1(\rho)-f_2(\rho)\right]\cos\delta\,\hat{\boldsymbol{z}}. \qquad \text{(II.12)}$$

In the following, we take $\gamma_n=-1.83247172\times10^4 s^{-1}G^{-1}$ as experimental value for the neutron gyromagnetic ratio.

Here, $C_m = \frac{4}{9}N'(0)k_F^2$ and $N'(0) = m_n^2/\left(2\pi^2 k_F\right)$ is the number density of states $N = m_n k/\left(2\pi^2\right)$ differentiated with respect to the energy $E = k^2/2m_n$ and evaluated at the Fermi surface $k = k_F$. For the numerical parameter values stated in Appendix A, $N'(0)$ takes the value $1.341\times10^{-5}\mathrm{MeV}^{-2}\mathrm{fm}^{-2}$ and C_m is computed to be $2.882\times10^{-5}\mathrm{MeV}^{-2}\mathrm{fm}^{-5}$. We display in Fig. 2 the resulting magnetization σ (II.12) for vanishing δ as a function of the rescaled distance $\tilde{\rho}$ from the vortex centre. The magnetization densities are evaluated using the vortex profile functions f_1, f_2 and g plotted in Fig. 1. Substituting the

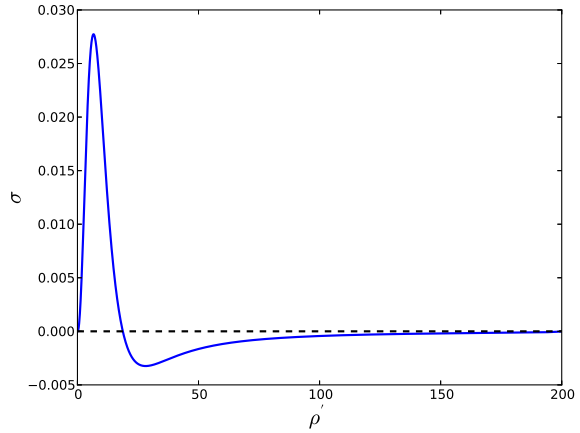

FIG. 2. Magnetization $\sigma(\tilde{\rho})$ for $\delta = 0$ plotted as a function of the rescaled distance $\tilde{\rho}$ from the vortex centre.

vortex profile functions computed for vanishing δ in (II.11), we can also find an estimate for the magnetization of the system as a function of δ. Integrating the magnetization (II.11) over the xy-plane gives the magnetic moment per unit length

$$\begin{aligned}\boldsymbol{m}(z) &= \frac{\gamma_n\hbar}{2}2\pi\xi^2\int\tilde{\rho}d\tilde{\rho}\boldsymbol{\sigma}(\tilde{\rho})\\ &= C_m\frac{|\alpha|}{6\beta}\frac{\gamma_n\hbar}{2}2\pi\xi^2\int\tilde{\rho}d\tilde{\rho}g(\tilde{\rho})(f_1(\tilde{\rho})-f_2(\tilde{\rho}))\cos\delta\,\hat{\boldsymbol{z}}.\end{aligned} \tag{II.13}$$

The integration in (II.13) can be performed numerically using the vortex profile function depicted in Fig. 1.
The integral is found to take the following value $2\pi\int\tilde{\rho}d\tilde{\rho}g(\tilde{\rho})(f_1(\tilde{\rho})-f_2(\tilde{\rho})) = -404.83$. Hence, for vanishing δ the magnetic moment per unit length is given by $m(z)\approx 4.196\times10^{-19}\mathrm{MeVfm}^{-1}\mathrm{G}^{-1}\approx 0.6\times10^{-27}\mathrm{JT}^{-1}\mathrm{fm}^{-1}$, which is one order less than the neutron magnetic moment.

III. THE LONG DISTANCE EFFECTIVE DESCRIPTION OF FREE ENERGY OF A VORTEX

In this section we discuss low energy effective description of excitations along a vortex line by using the so-called moduli approximation, originally used for monopoles [48] and applied to various topological solitons, e. g. Ref. [49]. At low energies, superfluid vortices can be characterized by Kelvin modes (two translational moduli). When orientating the vortex axis along the z-axis, these two moduli correspond to translations in the x- and y- direction. Physically these modes can be interpreted as the massless Nambu-Goldstone excitations generated from the spontaneous breaking of the translational symmetry. To compute the effective free energy for translational modes we substitute in the free energy functional (II.9) the vortex solution (II.4) which is shifted away from the origin by an amount $\boldsymbol{R}(z) = \{X_1, X_2\}$ with X_i $(i = 1,2)$ denoting the translational modes. In this case the order parameter is given by $A_{\mu i}(\boldsymbol{x}-\boldsymbol{R}(z))$. Note that the z-derivative of the order parameter gives a nonzero contribution to the free energy. The z-derivative of the order parameter is calculated via

$$\partial_z A_{\mu i} = -\frac{d\boldsymbol{R}(z)}{dz}\cdot\nabla A_{\mu i}. \tag{III.1}$$

Now, we can cast the resulting effective free energy in the following form

$$F_T = \mathscr{T}\int dz\; X_i'(z)^2, \tag{III.2}$$

where the prime denotes the derivative with respect to the coordinate z along the vortex. Here, the integral $\mathscr{T}$ measures the tension of the vortex and is given by

$$\begin{aligned}\mathscr{T} &= \frac{K}{G}\int \mathrm{d}^2 r\,\left\{|\partial_i A_{\mu j}|^2 + |\partial_i A_{33}|^2\right\}\\ &= \frac{2|\alpha|^2\xi^2}{G\beta}\int \mathrm{d}^2\tilde{\rho}\,\left\{\tilde{t}_1 + |\nabla(e^{i\theta}u)|^2\right\},\end{aligned} \tag{III.3}$$

where the energy density $\tilde{t}_1$ and the radial function u are defined in Sec. II B. The integral (III.3) is logarithmically divergent and can be approximately evaluated by inserting the asymptotic values of the profile functions as

$$\mathscr{T} \sim \frac{2\pi|\alpha|^2\xi^2}{G\beta}\log\frac{\Lambda_r}{\xi}, \tag{III.4}$$

where Λ_r is of the order of the system size for a single vortex. If there exists a vortex lattice, then Λ_r is of the order of the lattice spacing, that is of the order of μm.

Beside these translational modes we introduce a massive mode δ which may be important for understanding the spontaneous magnetization of the $^3P_2$ vortex. Interestingly, when

we switch on the mode δ in Eq. (II.11), the spontaneous magnetization changes inside the vortex core.

In this article we solved the equations of motion by imposing cylindrical symmetry, which makes the profile function independent of the z-coordinate. The parameter δ has been introduced as a constant. As we know, the vortex profile functions eventually reach their ground state value at large distances from the vortex core and $g(\rho)$ forms a concentric ring around the vortex and becomes practically zero outside the vortex, see Fig. 1. This is due to the ground state of the system being independent of δ. Therefore, we may treat δ as a collective coordinate (or a modulus) of a vortex and may take it as a function of z in the effective free energy functional. In principle, δ also depends on time but here we are not considering time dependence.

In our case, δ is a slowly varying function of the z-coordinate. Moreover, if we think of the vortices in the low energy approximation as thin strings , $\delta(t,z)$ can be treated as a field which lies on the two-dimensional string world sheet and fluctuations of δ may indicate changes in the magnetization on the world sheet.

The parameter δ depends on z and the z derivative of δ also contributes to the total effective energy. We insert the ansatz

$$A_\delta^{(\rho,\theta,z)} = e^{i\theta}\begin{pmatrix} f_1^0(\rho) & ig_0(\rho)e^{i\delta(z)} & 0 \\ ig_0(\rho)e^{i\delta(z)} & f_2^0(\rho) & 0 \\ 0 & 0 & -f_1^0-f_2^0 \end{pmatrix} \tag{III.5}$$

into the free energy functional (II.2) with the sixth order and magnetic term set to be zero and with the gradient and up to fourth order term given in Eqs. (II.3a) and (II.3b), respectively. With the ansatz (III.5) substituted into (II.2), the effective free energy takes the following form

$$F = \frac{4\alpha^2\xi^4}{\beta G}\int \mathrm{d}z\,\mathrm{d}^2\tilde{\rho}\left[\frac{1}{\xi^2}\left\{\left(\frac{2g_0}{\tilde{\rho}^2}(u_0-4v_0)+\frac{1}{\tilde{\rho}}(u_0g_0{}'-g_0u_0{}')\right)(\cos\delta-1)+\frac{g^2}{144}(u_0^2+v_0^2)(\cos 2\delta-1)\right\}+(\partial_z\delta)^2g_0^2\right], \tag{III.6}$$

where f_1^0, f_2^0 and g_0 are the vortex profile functions for zero δ, see Fig. 1. $u_0(\tilde{\rho})$ and $v_0(\tilde{\rho})$ are defined as $u_0 = f_1^0 + f_2^0$ and $v_0 = f_1^0 - f_2^0$, respectively. The rescaled radial distance $\tilde{\rho}$ is given by $\tilde{\rho} = \rho/\xi$, where ξ is the coherence length of the system. Eq. (III.6) can be expressed more neatly as,

$$F_{\text{eff}} = \int \mathrm{d}z\,\frac{4\alpha^2\xi^4}{\beta G}\left[\frac{1}{\xi^2}\{\lambda_1(\cos\delta-1)+\lambda_2(\cos 2\delta-1)\} + (\partial_z\delta)^2\lambda_3\right], \tag{III.7}$$

where the coefficients are defined as

$$\lambda_1 = \int d^2\tilde{\rho}\left(\frac{2g_0}{\tilde{\rho}^2}(u_0-4v_0)+\frac{1}{\tilde{\rho}}(u_0g_0'-g_0u_0')\right), \tag{III.8a}$$

$$\lambda_2 = \int d^2\tilde{\rho}\,\frac{g^2}{144}(u_0^2+v_0^2), \tag{III.8b}$$

$$\lambda_3 = \int d^2\tilde{\rho}\,g_0^2. \tag{III.8c}$$

The coefficients λ_1, λ_2 and λ_3 have been evaluated numerically to be given by

$$\lambda_1 = -4.889, \quad \lambda_2 = 0.411, \quad \lambda_3 = 17.748. \tag{III.9}$$

Note that the signs and numerical values of the λ coefficients are very important in this work. The graph of the effective potential (III.7) should exhibit a bump at the bottom because of the negative sign of the λ_2 contribution. However, as can be seen from Fig. 3, the minima occur at $\delta = 2\pi n$ with n being an integer. To get any local extrema other than $n\pi$, δ

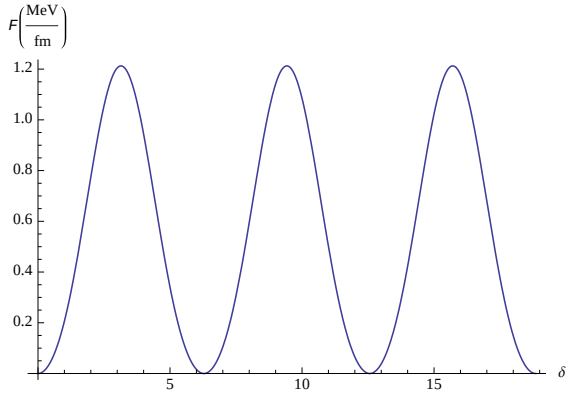

FIG. 3. We display the effective free energy potential F_{eff} (III.6) as a function of the δ parameter. We evaluate the free energy for the λ coefficients listed in Eq. (III.9). The GL parameters are given by $\alpha = -0.1$ and $\beta = 2.57664\,(\text{MeV fm})^{-2}$. The coherence length of the system is set to 30.3634 fm. Note that the energy values are given in units of MeV fm^{-1}.

has to satisfy the equation

$$\cos\delta = \frac{|\lambda_1|}{4\lambda_2}. \tag{III.10}$$

It can be checked that the numerically evaluated λ values (III.9) yield $\frac{|\lambda_1|}{4\lambda_2} > 1$. Hence, the obtained λ coefficients do not support any other local minima or maxima. This finding supports our expansion of the system around $\delta = 0$.

IV. DOUBLE SINE-GORDON KINK SOLUTION ON A VORTEX

In the last section, we have derived the effective free energy functional (III.7) that describes the low-energy dynamics of the system along with other dynamical terms. Since in this article we are solely interested in time independent configurations, we discuss in the following the static solutions of the system. Note that the system (III.7) is known as the double sine-Gordon model. However, the potential graph almost agrees with the sine-Gordon case because of the numerically calculated λ values (III.9), see Fig. 3. Here, we shall derive the kink solution and describe the physics behind the existence of the kink. We use the technique similar to Bogomol'nyi-Prasad-Sommerfield (BPS) monopoles [50, 51].

Let us rewrite the free energy (III.7) as,

$$F_{\rm eff} = \frac{4\alpha^2|\lambda_1|\xi^2}{\beta G}\int \mathrm{d}z\,\left[\left\{(1-\cos\delta)+\frac{\lambda}{2}(\cos 2\delta-1)\right\} + \frac{\xi^2\lambda_3}{|\lambda_1|}(\partial_z\delta)^2\right], \tag{IV.1}$$

where $\lambda = \frac{2\lambda_2}{|\lambda_1|}$. The numerical value of λ is evaluated to be 0.168735. After rescaling z, the effective free energy in Eq. (IV.1) takes the form

$$F_{\rm eff} = \frac{M_{\rm E}}{2}\int \mathrm{d}\zeta\,\left[\{2(1-\cos\delta)+\lambda(\cos 2\delta-1)\}+(\partial_\zeta\delta)^2\right], \tag{IV.2}$$

where $\zeta = \sqrt{\frac{|\lambda_1|}{2\lambda_3}}\frac{z}{\xi}$ and

$$M_E = \frac{4\alpha^2\xi^3\sqrt{2|\lambda_1|\lambda_3}}{\beta G}. \tag{IV.3}$$

Although the second term in Eq. (IV.2) is not positive, the potential part of Eq. (IV.2) is positive definite. So, we can use the BPS technique to find the kink solution. We write $F_{\rm eff}$ as,

$$F_{\rm eff} = \frac{M_E}{2}\int \mathrm{d}\zeta\,\left[\left\{\partial_\zeta\delta \pm \sqrt{2(1-\cos\delta)+\lambda(\cos 2\delta-1)}\right\}^2 + M_E\left|\partial_\zeta\delta\sqrt{2(1-\cos\delta)+\lambda(\cos 2\delta-1)}\right|\right]. \tag{IV.4}$$

Hence, $F_{\rm eff}$ satisfies the inequality

$$F_{\rm eff} \geq E_{\rm BPS} = M_E\left|\int d\zeta\,\partial_\zeta\delta\sqrt{2(1-\cos\delta)+\lambda(\cos 2\delta-1)}\right|. \tag{IV.5}$$

The minimum energy kink configuration saturates the energy bound (IV.5) and satisfies the so-called BPS equation

$$\partial_\zeta\delta = \pm\sqrt{2(1-\cos\delta)+\lambda(\cos 2\delta-1)}. \tag{IV.6}$$

It is easy to show that the solutions of the above equation also satisfy the original equation of motion derived from (III.6). The (anti)soliton solution of the BPS equation can be written as,

$$\delta(\zeta)\pm = \pi \pm 2\tan^{-1}\left(\Lambda\sinh\Lambda\zeta\right), \tag{IV.7}$$

where $\Lambda = \sqrt{1-2\lambda}$ is a real positive constant. It can be easily

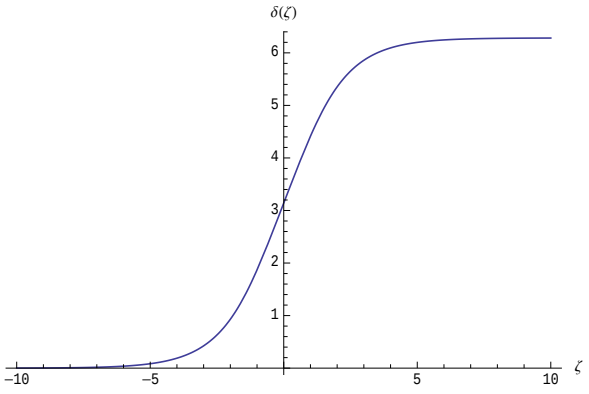

FIG. 4. The double sine-Gordon kink solution $\delta(\zeta)$ (IV.7) shown for $\Lambda = 0.813959$.

seen that for $\lambda = 0$, the above solution reduces to the usual sine-Gordon kink $\delta_{sG}(\zeta) = 4\arctan e^{\pm\zeta}$.

The BPS energy bound for the (anti)soliton can be expressed as

$$\begin{aligned} E_{\rm BPS} &= M_E\int_{\delta(-\infty)=0}^{\delta(\infty)=2\pi} d\delta\sqrt{2(1-\cos\delta)+\lambda(\cos 2\delta-1)} \\ &= \frac{M_E}{\sqrt{2\lambda}}\int_{-\sqrt{2\lambda}}^{\sqrt{2\lambda}} dt\sqrt{1-t^2} \\ &= 1.88\,M_E\,. \end{aligned} \tag{IV.8}$$

The total kink energy can be evaluated as

$$E_{\rm BPS} = 93.3\ \mathrm{MeV}\,. \tag{IV.9}$$

We display in Fig. 4 the double sine-Gordon kink solution $\delta(\zeta)$ obtained for the λ values given in Eq. (III.9). In Fig. 5, we plot the change in the vortex core magnetization in the presence of the kink solution along the z-axis. It is clearly observed that the magnetization changes its value continuously and reaches its opposite value at the center of the kink.

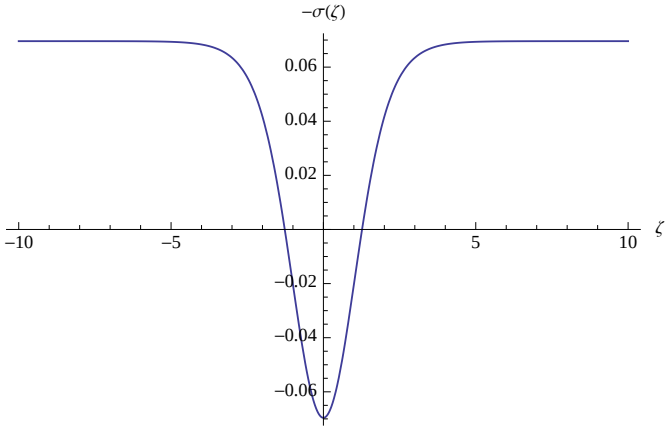

FIG. 5. The magnetization $\left(\frac{2m(\zeta)}{|\gamma_n|\hbar} = -\sigma(\zeta)\right)$ plotted as a function of the rescaled z-coordinate ζ.

V. CONCLUSIONS

In this article, we have derived a low energy effective theory of $^3P_2$ neutron superfluid vortices expressed solely in terms of the phase δ of the vortex profile function g. g lives in one of the off-diagonal components of the tensorial $^3P_2$ order parameter $A_{\mu i}$. Here, δ plays a crucial role as it gives a nonzero spontaneous magnetization in the core region of $^3P_2$ neutron superfluid vortices for the angular independent profile function g. Variations in δ change the induced magnetic moment accordingly. In our analysis we have found that at low energies the $^3P_2$ superfluid vortices are described by a double sine-Gordon model in addition to the well-known Kelvin (translational zero) modes part. We have derived a kink solution of this particular double sine-Gordon model and have determined its BPS energy bound. We have found that the vortex core magnetization flips its direction at the kink on the vortex.

Since the number of vortices in a rotating NS is of the order of 10^{19} and the NS radius is about 10 km, there should exist a large number of magnetic lumps in the NS interior like the ones discussed in this paper. At finite temperature, a pair of kink and anti-kink may be created spontaneously, and may trigger a phase transition inside the vortex. Possible implications of these objects for NS physics should be one of the most important future problems.

In this article, we have neglected higher order terms (esp. sixth order terms) in the GL free energy. We also did not take into account the effect of an external magnetic field. However, in the core of neutron stars where it is most likely to find neutron superfluid, the inclusion of high external magnetic fields and of the sixth order term would be important. So it would be interesting to study the effective free energy in the presence of high external magnetic fields and with nonzero sixth order term included. We have also considered only static configuration in this article. In order to discuss dynamics, we have to include time dependence. To this end, we need a time dependent GL equation, which has not been obtained yet. In the case of conventional superfluids, Kelvin modes will propagate with quadratic dispersion relation for small system sizes, see e. g. Ref. [52]. However, it is well known that for large system sizes the dispersion relation is given by $\varepsilon = k\log k$ with wave vector k. Recently, a formula for arbitrary system sizes has been obtained in Ref. [53]. On the other hand, the gapfull mode δ was previously unknown. We expect δ to have relativistic dynamics.

In this article, we have discussed only the integer vortex. For strong magnetic fields, the ground state is in the D_4-biaxial nematic phase admitting half-quantized non-Abelian vortices [43]. The vortex core magnetization is ten times larger than that of the integer vortex. For this case we should also derive the low-energy collective coordinate approximation and construct a magnetic lump.

ACKNOWLEDGEMENTS

This work is supported by the Ministry of Education, Culture, Sports, Science (MEXT)-Supported Program for the Strategic Research Foundation at Private Universities "Topological Science" (Grant No. S1511006). C. C. acknowledges support as an International Research Fellow of the Japan Society for the Promotion of Science (JSPS). Some of the work of M. H. was undertaken at the Department of Mathematics and Statistics, University of Massachusetts, financially supported by FP7, Marie Curie Actions, People, International Research Staff Exchange Scheme (IRSES-606096). The work of M. N. is supported in part by JSPS Grant-in-Aid for Scientific Research (KAKENHI Grant No. 25400268), and by a Grant-in-Aid for Scientific Research on Innovative Areas "Topological Materials Science" (KAKENHI Grant No. 15H05855) and "Nuclear Matter in Neutron Stars Investigated by Experiments and Astronomical Observations" (KAKENHI Grant No. 15H00841) from the the Ministry of Education, Culture, Sports, Science (MEXT) of Japan.

Appendix A: Ginzburg-Landau description for $^3P_2$ Superfluids

In this appendix, we briefly discuss the Ginzburg-Landau (GL) construction of $^3P_2$ superfluids and the associated GL parameter values. The Hamiltonian with $^3P_2$ contact interac-

tion can be written as

$$H = \int d^3\rho\ \psi^\dagger \left(-\frac{\boldsymbol{\nabla}^2}{2M} - \mu \right) \psi - \frac{1}{2} g T^\dagger_{\alpha\beta}(\boldsymbol{\rho}) T_{\alpha\beta}(\boldsymbol{\rho}), \tag{A.1}$$

$$T^\dagger_{\alpha\beta}(\boldsymbol{\rho}) = \psi^\dagger_\sigma(\boldsymbol{\rho})(t^*_{\alpha\beta})_{\sigma\sigma'}(\boldsymbol{\nabla})\psi^\dagger_{\sigma'}(\boldsymbol{\rho}), \tag{A.2}$$

where $\boldsymbol{\rho}$ denotes the space coordinates, ψ is a neutron field, μ is a baryon chemical potential, M is the neutron mass, and $g(>0)$ is the coupling constant. Here, α, β are the space indices, and the tensor $T_{\alpha\beta}$ represents the ${}^3P_2$ pair creation and annihilation operator. The differential operator t is defined as

$$(t_{\alpha\beta})_{\sigma\sigma'}(\boldsymbol{\nabla}) = \frac{1}{2}((S_\alpha)_{\sigma\sigma'}\nabla_\beta + \nabla_\alpha(S_\beta)_{\sigma\sigma'}) - \frac{1}{3}\delta_{\alpha\beta}(\boldsymbol{S})_{\sigma\sigma'} \cdot \boldsymbol{\nabla}, \tag{A.3}$$

and $\boldsymbol{S}$ is given by $(S_\alpha)_{\sigma\sigma'} = i(\sigma_y\sigma_\alpha)_{\sigma\sigma'}$ with $\alpha = x, y, z$ and pauli matrices σ.

The ${}^3P_2$ order parameter can be represented in general as a 3×3 traceless symmetric complex tensor $A_{\mu i}$, which is defined in Refs. [42, 45] as

$$\Delta = \sum_{\mu i} i\sigma_\mu \sigma_y A_{\mu i} k_i, \tag{A.4}$$

where Δ is the gap parameter. As above, Latin subscripts stand for spin indices while Roman indices denote the spatial coordinates. The tensor $A_{\mu i}$ is related to $T_{\alpha\beta}$ as given in Ref. [22],

$$A_{\alpha\beta} = g\langle T_{\alpha\beta}(\boldsymbol{\rho})\rangle_T, \tag{A.5}$$

where the angular brackets are defined as an ensemble average in the grand canonical ensemble.

In Table I, we summarise the coefficients α, β, K_1 and K_2 (the GL parameters) calculated in the weak coupling limit by considering only the excitations around the Fermi surface [22, 45, 46]. In this limit, K_1 and K_2 in Eq. (II.3a) take the same value. To simplify comparison with the works [22, 42, 43], we fix the numerical values of our model parameters as discussed in the following. We assume a nuclear mass density of $\rho_n = 6\times 10^{17}\,\mathrm{kg\,m^{-3}}$ [22] and a neutron mass $\mathrm{M}_n = 1.67\times 10^{-27}$ kg. Hence, the number density of nucleons in a nucleus is roughly given by $n = \rho_N/\mathrm{M}_n = 0.359\,\mathrm{fm}^{-3}$. This results in a Fermi momentum of $k_F = (3\pi^2 n)^{1/3} = 2.1987\mathrm{fm}^{-1}$. Defining $\mathrm{m}_n = \mathrm{M}_n c^2/\left(\hbar^2 c^2\right) = 0.02413\,\mathrm{MeV}^{-1}\mathrm{fm}^{-2}$ with $\mathrm{M}_n c^2 = 939.57\mathrm{MeV}$, we can calculate the fermi energy via $\varepsilon_F = k_F^2/(2\mathrm{m}_n) = 100.172\,\mathrm{MeV}$. With the numerical values for m_n and k_F stated above, the number density of states on the Fermi surface at $k = k_F$ is computed to be $N(0) = \mathrm{m}_n k_F/\left(2\pi^2\right) = 0.002688\,\mathrm{MeV}^{-1}\mathrm{fm}^{-3}$. Furthermore, in the calculation of the GL parameters (see Table I) we assume that the transition to the neutron ${}^3P_2$ superfluid phase occurs at the critical temperature value $T_C = 0.2\,\mathrm{MeV}$ and $T = 0.8T_C$. . The Riemann ζ function $\zeta(n)$ is defined by $\zeta(n) = \sum_{k=1}^{\infty} k^{-n}$. Hence, $\zeta(3) = 1.202$.

Appendix B: Equations of Motion

In this appendix, we list explicitly all the vortex equations together with the imposed boundary conditions. Note that all vortex equations are given in the cylindrical basis ($n = 1$).

The equations of motion derived from (III.2) are given by

$$\tilde\rho^2\left(4u''+v''\right) + \tilde\rho(4u'+3v'-4g') - (4u-v+4g) - \frac{\tilde\rho^2}{144}\left(\frac{36\alpha}{|\alpha|} + 9u^2 + 3v^2 + 20g^2\right)u = 0, \tag{B.1a}$$

$$\tilde\rho^2\left(u''+2v''\right) + \tilde\rho\left(2v'-u'\right) - (10v-u-16g) - \frac{\tilde\rho^2}{144}\left(\frac{12\alpha}{|\alpha|} + 3u^2 + v^2 + 12g^2\right)v = 0, \tag{B.1b}$$

$$4\tilde\rho^2 g'' + 2\tilde\rho(2g'+u') + 2(4v-u-10g) - \frac{\tilde\rho^2}{72}\left(\frac{12\alpha}{|\alpha|} + 5u^2 + 3v^2 + 4g^2\right)g = 0. \tag{B.1c}$$

All profile function u, v and g are required to vanish at the origin. At spatial infinity we impose the following boundary conditions which are compatible to the above equations of motion

$$u^2 = (f_1+f_2)^2 = \frac{6}{(r^2+(1+r)^2+1)}, \tag{B.2a}$$

$$v^2 = (f_1-f_2)^2 = \frac{6(2r+1)^2}{(r^2+(1+r)^2+1)}, \tag{B.2b}$$

$$u' = v' = g' = g = 0. \tag{B.2c}$$

Hence, with the vortex boundary state selected to be given by the lowest energy state $r = -0.557$ (due to the fourth order term), the linear combinations $u = f_1 + f_2$ and $v = f_1 - f_2$ have to fullfill the boundary conditions $u(\infty) = 1.9956$ and $v(\infty) = 0.2275$.

[1] A. W. Steiner, J. M. Lattimer, and E. F. Brown, Astrophys. J. **765**, L5 (2013).

[2] J. M. Lattimer and M. Prakash, Phys. Reps. **442**, 109 (2007), The Hans Bethe Centennial Volume 1906-2006.

α	$K_1 = K_2$	β
$\frac{T-T_c}{2T_c}$	$\frac{7\zeta(3)}{240M_n^2}\frac{N(0)G}{(\pi T_c)^2}k_F^4$	$\frac{7\zeta(3)}{60}\frac{N(0)G}{(\pi T_c)^2}k_F^4$
-0.1	$1106.32\ \mathrm{fm}^2$	$2.57664\ (\mathrm{MeV\ fm})^{-2}$

TABLE I. Summary of the GL parameters computed in the weak coupling limit. Note that in this limit K_1 and K_2 are set to be equal. Recall that we take $g'_H = 0$ in Eq. (II.3d). In this article, the GL parameters have been computed for a critical temperature value $T_C = 0.2\,\mathrm{MeV}$, temperature $T = 0.8T_C$, neutron mass $\mathrm{M}_n c^2 = 939.57\mathrm{MeV}$, Fermi momentum $k_F = 2.1987\mathrm{fm}^{-1}$, rescale parameter $G \approx 115.39\,\mathrm{MeV\,fm}^5$, number density of states $N(0) = 0.00268815\,\mathrm{MeV}^{-1}\mathrm{fm}^{-3}$. The Riemann ζ function takes the value $\zeta(3) = 1.202$. We refer the reader to the last paragraph of section A for the numerical values of all model parameters used in our numerical simulations.

[3] N. Chamel and P. Haensel, Living Rev. Rel. **11** (2008).

[4] *Lecture Notes for the NATO Advanced Study Institute on Timing Neutron Stars*, NATO ASI Series C, Vol. 262 (Kluwer Academic Press, 1989) held in Cesme, Turkey.

[5] D. Page, M. Prakash, J. M. Lattimer, and A. W. Steiner, Phys. Rev. Lett. **106**, 081101 (2011).

[6] P. S. Shternin, D. G. Yakovlev, C. O. Heinke, W. C. G. Ho, and D. J. Patnaude, Month. Not. Roy. Astr. Soc. **412**, L108 (2011).

[7] L. B. Leinson, Phys. Lett. **B741**, 87 (2015).

[8] D. Pines, J. Shaham, and M. Ruderman, Nature Phys.Sci. **237**, 83 (1972).

[9] T. Takatsuka and R. Tamagaki, Prog. Theor. Phys. **79**, 274 (1988).

[10] G. Baym, C. Pethick, D. Pines, and M. Ruderman, Nature **224**, 872 (1969).

[11] P. W. Anderson and N. Itoh, Nature **256**, 25 (1975).

[12] M. Ruderman, Astrophys. J. **203**, 213 (1976).

[13] D. Pines and M. Ali Alpar, Nature **316**, 27 (1985).

[14] G. Baym and D. Pines, Ann. Phys. **66**, 816 (1971).

[15] M. A. Alpar, H. F. Chau, K. S. Cheng, and D. Pines, Astrophys. J. **459**, 706 (1996).

[16] G. Baym, C. Pethick, and D. Pines, Nature **224**, 673 (1969).

[17] R. Tamagaki, Prog. Theor. Phys. **44**, 905 (1970).

[18] M. Hoffberg, A. E. Glassgold, R. W. Richardson, and M. Ruderman, Phys. Rev. Lett. **24**, 775 (1970).

[19] T. Takatsuka and R. Tamagaki, Prog. Theor. Phys. **46**, 114 (1971).

[20] T. Takatsuka, Prog. Theor. Phys. **47**, 1062 (1972).

[21] T. Fujita and T. Tsuneto, Prog. Theor. Phys. **48**, 766 (1972).

[22] R. W. Richardson, Phys. Rev. **D5**, 1883 (1972).

[23] N. D. Mermin, Phys. Rev. **A9**, 868 (1974).

[24] J. A. Sauls and J. W. Serene, Phys. Rev. **D17**, 1524 (1978).

[25] J. L. Song, G. W. Semenoff, and F. Zhou, Phys. Rev. Lett. **98**, 160408 (2007).

[26] S. Uchino, M. Kobayashi, M. Nitta, and M. Ueda, Phys. Rev. Lett. **105**, 230406 (2010).

[27] K. Masuda and M. Nitta, Phys. Rev. **C93**, 035804 (2016).

[28] T. Mizushima, K. Masuda, and M. Nitta, (2016), arXiv:cond-mat.supr-con/1607.07266.

[29] V. Z. Vulovic and J. A. Sauls, Phys. Rev. **D29**, 2705 (1984).

[30] P. F. Bedaque, G. Rupak, and M. J. Savage, Phys. Rev. **C68**, 065802 (2003).

[31] P. F. Bedaque and A. N. Nicholson, Phys. Rev. **C87**, 055807 (2013), [Erratum: Phys. Rev. **C89**, no.2, 029902 (2014)].

[32] P. F. Bedaque, A. N. Nicholson, and S. Sen, Phys. Rev. **C92**, 035809 (2015).

[33] L. B. Leinson, Phys. Rev. **C81**, 025501 (2010).

[34] L. B. Leinson, Phys. Lett. **B689**, 60 (2010).

[35] L. B. Leinson, Phys. Rev. **C82**, 065503 (2010), [Erratum: Phys. Rev. **C84**, 049901 (2011)].

[36] L. B. Leinson, Phys. Rev. **C83**, 055803 (2011).

[37] L. B. Leinson, Phys. Rev. **C84**, 045501 (2011).

[38] L. B. Leinson, Phys. Rev. **C85**, 065502 (2012).

[39] L. B. Leinson, Phys. Rev. **C87**, 025501 (2013).

[40] K. M. Shahabasyan and M. K. Shahabasyan, Astrophysics **54**, 429 (2011).

[41] P. Muzikar, J. A. Sauls, and J. W. Serene, Phys. Rev. **D21**, 1494 (1980).

[42] J. A. Sauls, D. L. Stein, and J. W. Serene, Phys. Rev. **D25**, 967 (1982).

[43] K. Masuda and M. Nitta, (2016), arXiv:nucl-th/1602.07050.

[44] Sine-Gordon kinks on vortices were studied in the Skyrme model [54, 55]. In this case, the kink represents a Skyrmion, carrying a non-zero baryon number.

[45] T. Fujita and T. Tsuneto, Prog. Theor. Phys. **49**, 371 (1973).

[46] J. A. Sauls, *Anisotropic Superfluidity in Neutron Stars and Strong Coupling Effect in Superfluid ^{3}He, Ph.D. Thesis, SUNY, Stony Brook.* (1980).

[47] S. Kobayashi, Y. Kawaguchi, M. Nitta, and M. Ueda, Phys. Rev. **A86**, 023612 (2012).

[48] N. S. Manton, Phys. Lett. **B110**, 54 (1982).

[49] M. Eto, Y. Isozumi, M. Nitta, K. Ohashi, and N. Sakai, Phys.

Rev. **D73**, 125008 (2006).
[50] E. B. Bogomolny, Sov. J. Nucl. Phys. **24**, 449 (1976), [Yad. Fiz. 24, 861 (1976)].
[51] M. K. Prasad and C. M. Sommerfield, Phys. Rev. Lett. **35**, 760 (1975).
[52] M. Kobayashi and M. Nitta, PTEP **2014**, 021B01 (2014).
[53] D. A. Takahashi, M. Kobayashi, and M. Nitta, Phys. Rev. **B91**, 184501 (2015).
[54] S. B. Gudnason and M. Nitta, Phys. Rev. **D90**, 085007 (2014).
[55] S. B. Gudnason and M. Nitta, Phys. Rev. **D94**, 025008 (2016).